communications biology

A Nature Portfolio journal

Article

https://doi.org/10.1038/s42003-025-08169-7

Neural representation of self-initiated locomotion in the secondary motor cortex of mice across different environmental contexts

Guanglong Sun[1,2,3,4,10], Chencen Yu[1,10], Ruolan Cai[1,10], Mingxuan Li[5], Lingzhu Fan[1], Hao Sun[1,6], Chenfei Lyu[1], Yingxu Lin[1,6], Lixia Gao[1,2,4,6], Kuan Hong Wang[7,8,11] ✉ & Xinjian Li[1,4,7,9,11] ✉

The secondary motor cortex (M2) plays an important role in the adaptive control of locomotor behaviors. However, it is unclear how M2 neurons encode the same type of locomotor control variables in different environmental contexts. Here we image the neuronal activity in M2 with a miniscope while mice are moving freely in each of three environments: a Y-maze, a running-wheel, and an open-field. These animals show distinct locomotor patterns in different environmental contexts. Surprisingly, a large population of M2 neurons are active before starting and after ceasing locomotion, while maintaining decreased neural activity during locomotion. Furthermore, the majority of these neurons are consistently engaged across various contexts, suggesting egocentric voluntary control functions. In contrast, the smaller populations of locomotion-activated M2 neurons are mostly context-specific, suggesting exocentric navigation functions. Thus, our results demonstrate that M2 neurons encode motor control variables for self-initiated locomotor behaviors in both context-dependent and context-independent manners.

Self-initiated locomotion is a fundamental behavior that allows animals to move from one place to another and interact with their surrounding environments[1,2]. Typically, locomotion is divided into several stages, such as locomotor initiation, termination, maintenance, and steering[3]. To control the musculature associated with locomotion, various parts of the central nervous system have to determine when, where, and how to move[1,3,4]. Neural circuits in the spinal cord determine how to execute locomotor movements, such as limb coordination, step patterns, and movement speed[5]. The signals to start, maintain and stop movement have been found in reticulospinal, midbrain, and striatal circuits[4,6], which determine when to move. Turning, navigation, and goal-related "where" signals are controlled by cortical-basal ganglia-thalamocortical loops[7,8]. Although the neural control of locomotion has been extensively investigated and enabled brain-machine interface design[9,10], most efforts have been devoted to determining the neural mechanisms underlying locomotor control in a single environmental context. However, an unsolved issue is how neurons encode the same type of locomotor control variables in different environmental contexts. Lack of this knowledge has impeded the development of a generalizable brain-machine interface.

Among the motor-related brain regions, the motor cortex[11], including the secondary motor cortex (M2), is a key region for controlling voluntary and adaptive locomotion[12]. The rodent M2 cortex is functionally analogous to the primate and feline premotor cortex[13–17] and is an important hub for the planning and control of motor function. M2 receives diverse sensory inputs[18] and broadcasts motor control signals through long-range projections to multiple motor areas along the neuraxis[19], suggesting that sensory input can influence M2 activity and locomotor behaviors[20–26]. In addition, deep-layer M2 neurons project to the spinal cord *via* the corticospinal tract and send out command signals to precisely control skilled voluntary action[19,27–29] and locomotion[3]. Extensive studies have revealed that M2 neural activity precedes downstream targets in cue-triggered motor response selection tasks[12,30]. However, how M2 neurons encode multiple movement-related variables during self-initiated locomotion in different environmental contexts remains unknown. Since motor planning is a fundamental function of the M2 cortex, we hypothesize that the neural processing underlying start/stop actions remains consistent across different contexts. In contrast, neural processing associated with locomotion and speed control—both of which can be modulated by sensory input—is likely to vary significantly between environmental contexts.

A full list of affiliations appears at the end of the paper. ✉e-mail: kuanhong_wang@urmc.rochester.edu; lxjbio@zju.edu.cn

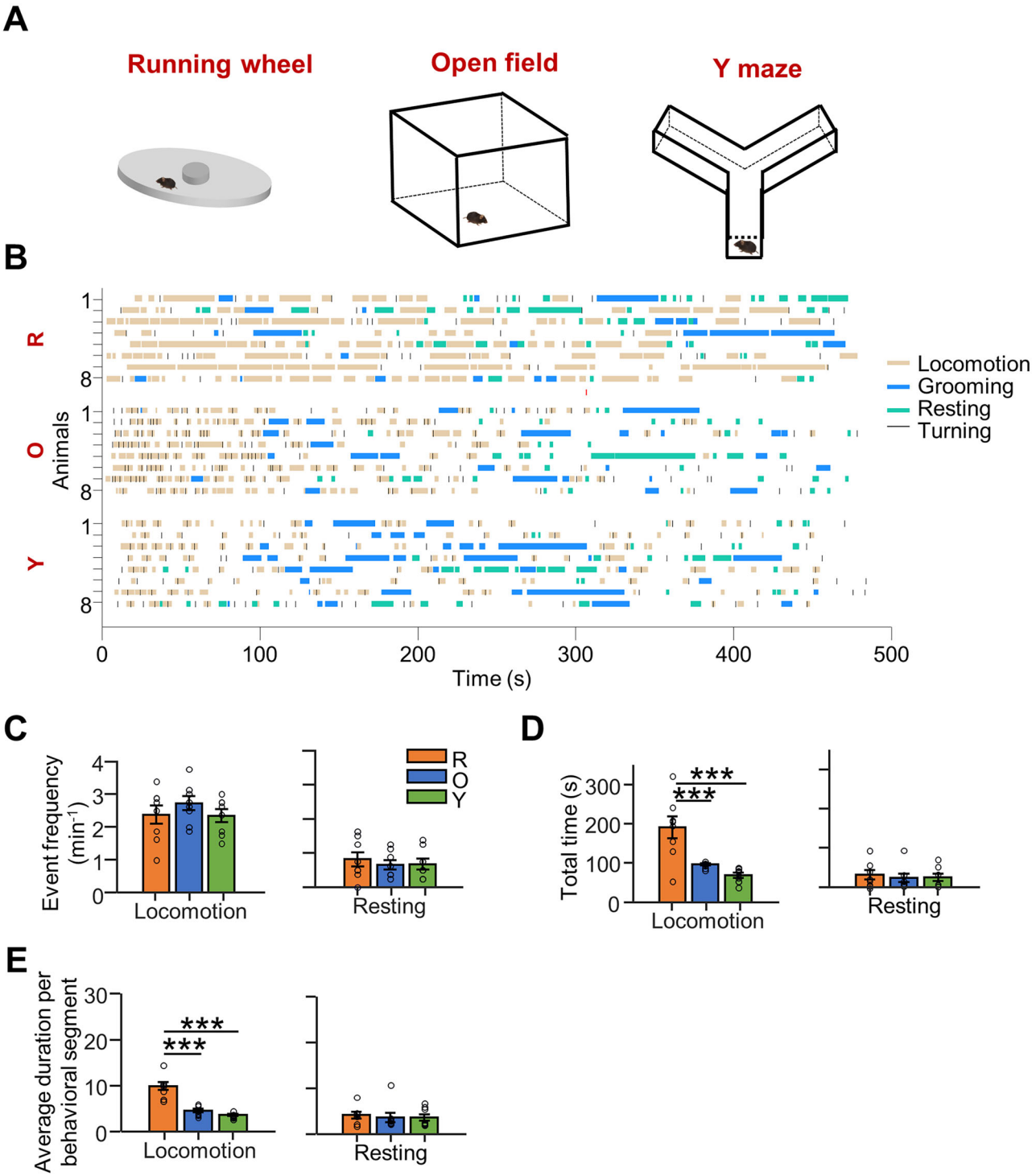

Fig. 1 | Characterization of mouse movement patterns in three different environmental contexts. A Diagrams showing locomotor behaviors in 3 environmental contexts. Left, running wheel; middle, open field; right, Y maze. **B** Human-defined locomotor behaviors during 8 min of free movement in the three contexts. The animal's behavior was defined frame by frame. Each labeled segment of locomotion, grooming, or resting lasts >2 s without any other kinds of interrupting behaviors. To meet the definition of turning, the animal must run straight forward first, then make a turn followed by another straight run; and the angle of each turn must be >30°. Unlabeled gaps correspond to periods when animal's behavior patterns do not fit into the above categories, often due to small body movements. R, running wheel; O, open field; Y, Y maze (same below). The frequency of locomotion (**C**) and rest (**D**) in the 3 contexts (min^{-1}). $N = 8$ biologically independent animals. Locomotion: $F = 0.805$, $p = 0.462$; Resting: $F = 0.266$, $p = 0.769$. Total time of locomotion (**E**) and rest (**F**) in the 3 contexts. $N = 8$ biologically independent animals. Locomotion: $F = 14.790$, $p < 0.001$; Resting: $F = 0.169$, $p = 0.845$. The average duration of locomotion (**G**) and rest (**H**) segments in 8 min of testing in the 3 contexts. $N = 8$ biologically independent animals. Locomotion: $F = 38.336$, $p < 0.001$; Resting: $F = 0.122$, $p = 0.886$. $^{*}p < 0.05$, $^{**}p < 0.01$, $^{***}p < 0.001$, one-way ANOVA followed by LSD test for multiple comparisons. Error bars represent the standard error.

In the current study, we placed mice into three behavioral contexts to examine the neural representation of self-initiated locomotion: the Y-maze, running wheel, and open field. The animals showed start, stop, running, and resting behaviors in those contexts. Then, through Ca^{2+} imaging in M2, we addressed how M2 encodes self-initiated locomotion across different contexts. We found that the locomotor start/stop-related signals in M2 spanned different contexts, which may represent egocentric voluntary motor control functions less modulated by the environment. In contrast, the locomotion-maintenance neurons were more context-specific, suggesting exocentric locomotor navigation functions. Thus, our results demonstrated that M2 encodes locomotion control variables in both context-dependent and independent manners.

Results

Characterization of mouse movement patterns in three different environmental contexts

To adapt to different environments, animals have to exhibit distinct patterns of behavior, including locomotion. However, it is unclear how M2 neurons are modulated during self-initiated locomotor behaviors in different environmental contexts. To address this question, animals were placed in three distinct environmental contexts, a Y-maze, a running wheel, and an open field, and were allowed to freely explore these contexts for 8 min (Fig. 1A). Different behavior patterns, including locomotion, grooming, and resting, were manually annotated using video recordings (Fig. 1B; see Methods). Each labeled segment of locomotion, grooming, and resting behavior had to exceed 2 s (details in Methods). Some short video segments that included multiple behaviors or did not meet the criteria were excluded from the analysis and presented as unlabeled gaps (Fig. 1B). We found no significant difference in the number of locomotion segments over the 8-minute period (Fig. 1C). However, the total (Fig. 1E) and segment-averaged locomotion time (Fig. 1G) were significantly longer in the running wheel than in the open field and Y-maze. There was no difference in resting time or frequency between the three contexts (Fig. 1D, F, H). To alternatively assess the animals' behavior, locomotion and resting behavior were also defined by automatic methods based on motion tracking. We found that the animals still showed longer locomotion in the running wheel than in the open field and Y-maze (Supplementary Fig. 1). Thus, mice exhibit different locomotor patterns in different behavioral contexts.

Classifying locomotion-related neural activity by fitting second-order polynomial functions

To study how M2 neurons encode self-initiated locomotion, AAV-hSyn-GCaMP6s, a fluorescent Ca^{2+} indicator, was infused into the superficial layers of M2 using our previously published method[31] (Fig. 2A–C). With this method, we primarily labeled neurons in the superficial layers (layers 2/3) of the M2 region (Fig. 2D). Two weeks after virus infusion, the M2 activity was imaged using a miniature fluorescence microscope in freely moving mice in different behavioral contexts (Fig. 2A, B). We checked the raw ΔF/F traces of the imaged neurons (Supplementary Fig. 2A–C) and confirmed that they displayed a typical calcium activity profile characterized by a rapid rise phase followed by a slow decay phase (Supplementary Fig. 3C). The rising phase was used to define calcium events, which correlate with neuronal spike activity, as shown in previous studies[32].

To examine the neural correlates of locomotor behavior, neural activity traces were usually aligned to a specific locomotor event and then the mean activity before and after the event was compared to evaluate event-related changes[19,33]. This method works well in simple cue-triggered locomotion or sensory tasks, where sensory cues are delivered by the experimenter and neural responses occur after cue onset. However, for self-initiated locomotion, event-related neural changes may ramp up or down around a specific time point. A straightforward before-and-after comparison based on a step function would fail to capture this type of complex neural dynamics. Indeed, when we aligned the calcium activity across different trials by a specific locomotor event, such as locomotion start (Fig. 2E), we observed several consistent neural activity profiles across different trials. Some neurons showed peak activity prior to the locomotor event (Pre), some around the locomotor event (Onset(+)), and some after the locomotor event (Post). Additionally, some neurons showed peak activity both before and after the locomotor event (Onset(−)) (Fig. 2E).

To better characterize such dynamic and diverse activity patterns of M2 neurons during self-initiated locomotion, we used second-order polynomial functions to fit the neural activity of individual neurons around locomotion events (Fig. 2F; Methods), adapting a method from a previous study[34]. To illustrate this analysis method with the neural data from a representative animal, we aligned the activity of each neuron to the onset of locomotion and averaged the activity across trials. Then, we established a threshold requiring at least 50% of trials to exhibit locomotion-related responses to remove unstable neurons. As a result, this analysis removed 20–30% of neurons. The trial-averaged neuronal activity of the remaining neurons (Fig. 2F, gray curve) was fitted with a second-order polynomial function (Fig. 2F, dashed curve). Given that the motor cortex typically sends a command signal 0.2–0.3 s prior to the movement onset to control voluntary movement[19,27–29], we used a 0.3 s window before and after movement onset to define the M2 activity. According to the shape and location of the fitted curves, which were jointly determined by the quadratic and linear coefficients of the second-order polynomial function, the neurons were classified into 4 groups: Pre, onset(+), onset(−), and Post (Fig. 2F, G, Table 1, Methods). The maximal activity of Pre neurons fell in the window of 0.3–1.5 s before the locomotion start, while the maximal activity of Post neurons was 0.3–1.5 s after the locomotion start. The neurons of onset (+) and onset(−) displayed maximal or minimal activity between −0.3 and 0.3 s (Fig. 2F, H–I). Notably, there was a larger population of Pre neurons compared to other groups in the example animal during the time window of locomotion start (Fig. 2H, J). In addition, the neural activity patterns within the same group showed high temporal similarity (Fig. 2K, diagonal red blocks). Finally, neurons from different groups were spatially mapped onto the cortical locations of M2 and were found to be intermixed (Fig. 2L).

To compare the second-order polynomial function-based classification scheme with an alternative method, we classified the neurons by comparing the average neural activity in different time windows. We found that the neurons could be grouped into similar categories (Supplementary Fig. 2E), with each group exhibiting comparable response patterns (Supplementary Fig. 2F) and similar population percentages to those classified using second-order polynomial functions (Supplementary Fig. 2G). Thus, the activity patterns of M2 neurons were robustly classified with second-order polynomial functions.

Active M2 neurons before and after locomotion are over-represented across contexts

Animals' behavior in the three environments can switch from one state to another, e.g., from resting to locomotion, from locomotion to resting, turning, etc. To understand how M2 neurons are involved in behavioral switching, we aligned the M2 activity of 8 mice by locomotion start (LST) (Fig. 3A and Supplementary Fig. 3A), averaged each neuron's activity across trials, and then classified the activity profile using the second-order polynomial functions. The neurons were sorted based on the timing of each cell's peak activity in odd-numbered trials of the Y maze. This sorting order was then applied to the average activity from the even-numbered trials to validate the consistency of response patterns within the same context. The same order was also used for all trials in the open field and running wheel conditions, allowing for consistent comparison across contexts (Fig. 3B). Furthermore, cells were grouped into three categories based on their ability to represent across contexts: cross-three-context neurons, cross-two-context neurons, and single-context neurons. Using this approach, we found that a large proportion of neurons were active before the LST in each context, and some of them were active across all three or two contexts (Fig. 3B). To further evaluate the response stability of M2 neurons, we split each recording session into two halves. The sequence of cells in the second half was identical to that in the first half. We found that most cells remained in the same response category across both halves of the trials. For example,

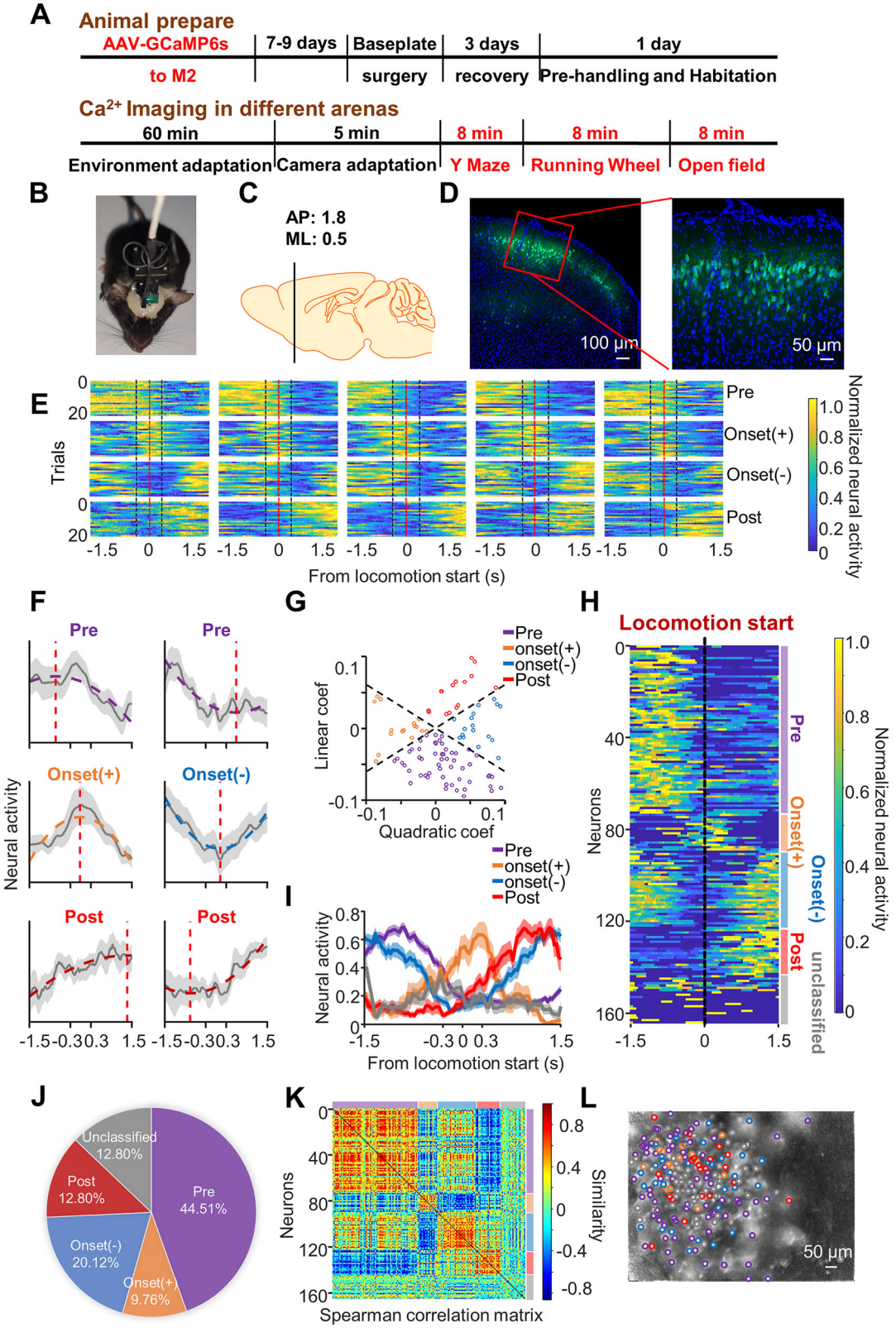

most Pre neurons in the first half were also classified as Pre in the second half (Supplementary Fig. 4A). Compared to randomly shuffled data, the increased percentage of neurons exhibiting the highest activity 0.3–1.5 s before LST [Pre] was significant across all three contexts (Fig. 3C). However, the increased percentage of neurons with the highest activity from −0.3 to 0.3 s during LST [onset(+)] was only significant in the running wheel and open field contexts (Fig. 3C). In addition, shuffling neural activity resulted in a greater proportion of unclassified neurons, as expected due to the disruption of structured neural patterns (Fig. 3C).

We then asked whether the over-represented neural activity before LST in M2 neurons could be consistently observed across different contexts. Interestingly, we found that some neurons (12.76 ± 1.96%) showed similar

Fig. 2 | Classification of neuronal activity patterns by fitting second-order polynomial functions. A Upper: Schematic of the experimental procedure. Lower: Schematic of the Ca^{2+} imaging procedure in the 3 contexts. **B** Representative Ca^{2+} imaging with a miniature microscope in a freely-behaving mouse. **C** Sketch showing the viral labeling region. **D** Confocal fluorescent image of a coronal section showing labeled neurons using the surface-based viral (AAV2/9-hSyn-GCaMP6s, green) infusion method. **E** Raster plots showing the activities of representative Pre, onset (+), onset(−), and Post neurons (5 example neurons per category) aligned by locomotion start across trials. Y axis indicates trial numbers. **F** Examples of Pre, onset(+), onset(−), and Post neurons during locomotor behaviors. The activity of each neuron was first aligned by the start of locomotion and averaged across trials (gray curve). The average neuronal activity was fitted with a second-order polynomial function (dashed curve). Continuous and dashed lines show the observed neural activity trace and its corresponding quadratic curve fit, respectively. Vertical red dashed lines indicate the time when the fitted quadratic curves reach either maximum or minimum activity levels. If the fitted quadratic curve opened downward (negative quadratic coefficient) and the maximum activity was reached in the window from −1.5 s to −0.3 s, or if the fitted quadratic curve opened upward (positive quadratic coefficient) and the minimum activity was reached in the window from 0.3 s to 1.5 s, the neuron was defined as a Pre neuron. If the quadratic curve opened downwards and the maximum was reached in the window from 0.3 s to 1.5 s, or if the quadratic curve opened upwards and the minimum was reached in the window from −1.5 s to −0.3 s, the neuron was defined as a Post neuron. If the quadratic curve opened downwards and the maximum was reached from −0.3 s to 0.3 s, the neuron was defined as an onset(+) neuron. If the quadratic curve opened upwards and the minimum was reached between −0.3 s and 0.3 s, the neuron was defined as an onset(−) neuron. **G** Scatterplot of the linear (y-axis) and quadratic (x-axis) coefficients of the fitted 2nd order polynomial functions for all neurons of an example animal in the open field context. The two dashed lines ($y = 0.6x$ and $y = -0.6x$) divide the parameter space into four sectors according to the criteria specified in (**F**). **H** Raster plot showing the activity of 164 neurons aligned by the start of locomotion in an example animal. The neurons were sorted in the sequence Pre, onset(+), onset(−), Post, and unclassified. **I** Averaged activity of Pre, onset(+), onset(−), and Post neurons. **J** Percentage of Pre, onset(+), onset(−), and Post neurons during the window of locomotion start in the example animal. **K** Pair-wise correlation of 164 neurons sorted in the same sequence as in (**H**). **L** Spatial distribution of different types of neurons.

Table 1 | Functional classification criteria for neuronal start/stop/turn related signals

Criteria				$p < 0.05$				$p > 0.05$
	a > 0			a < 0				
(−b/2a)	>0.3	[−0.3,0.3]	<−0.3	>0.3	[−0.3, 0.3]	<−0.3	Active time <0.5	–
Classification	pre(+)	onset(−)	post(+)	post(+)	onset(+)	pre(+)	unclassified	unclassified

activation patterns across all 3 behavioral contexts, and some neurons (49.54 ± 1.83%) in 2 contexts, while the others displayed diverse activity in different contexts (Fig. 3D). Then, we examined the spatial distribution of different groups of neurons and found that single and cross-context neurons were mixed together (Supplementary Fig. 3B–E). To further explore whether the cross-context neurons occur randomly in the M2 region, we shuffled the neural activity of M2 and calculated cross-context neurons in the shuffled dataset (see Methods). Compared to the shuffled data, there were fewer single-context cells (Fig. 3D) but more three-context and two-context cells (Fig. 3D). Moreover, most two-and three-context neurons were Pre and their proportions were significantly higher than that in the shuffled population (Fig. 3E, F). The proportions of other groups of neurons were not different from the chance level in the shuffled data (Fig. 3E, F). In addition, the average activity profiles of these cross-context cells showed that they were active before locomotion start (Fig. 3G). Taken together, these results suggest that a large proportion of M2 neurons are active before locomotion start and the same neurons are activated similarly across environmental contexts.

Next, we analyzed the M2 activity around the locomotion stop (LSP) with the second-order polynomial functions (Fig. 4A). After splitting each recording session into two halves of trials, we found that most cells remained in the same response category across both halves. For instance, the majority of Post neurons in the first half were also classified as Post in the second half (Supplementary Fig. 4B), indicating the response stability of M2 neurons when their activity was aligned with LSP. In addition, we found that most neurons displayed the highest activity 0.3–1.5 s after LSP [Post] in the 3 contexts (Fig. 4B, C), which was distinct from the observation of more Pre neurons around LST (Fig. 3). Compared to randomly shuffled data, the increased percentage of Post cells was significant in all three environmental contexts (Fig. 4C). We then asked whether the over-represented neural activity after LSP in M2 neurons could be consistently observed across different contexts. Interestingly, we found that some neurons showed similar activation patterns in all 3 contexts, and some across 2 contexts, while the others displayed diverse activity in different contexts (Fig. 4D). Most two-and three-context neurons were Post and onset(+) and their proportions were significantly higher than that in the shuffled population (Fig. 4E, F). Although the activity of those cross-context neurons tended to peak 0.3–1.5 s after LSP, they started to activate before LSP (Fig. 4G). Thus, these neurons could modulate stopping behaviors during locomotion. Altogether, M2 neurons that are active before and after locomotion are over-represented across contexts, suggesting that they may play a crucial role in controlling the initiation and cessation of self-initiated locomotion.

M2 neurons show more sustained suppression than activation during linear locomotion

Apart from locomotion start- or stop-related behavior switching, other behavioral patterns in the three environments persisted for a while, such as linear locomotion and resting. Therefore, we assessed whether M2 neurons would show similar activity patterns during sustained locomotion in different contexts. Because the duration of each self-initiated locomotion trial was variable, the activity of individual neurons across different trials was first interpolated to 120 standardized sample points, corresponding to the median trial duration of 4 s at a sampling rate of 30 Hz. This interpolation enabled consistent averaging across trials. In addition, 45 sample points (1.5 s) of activity before and after locomotion were included to provide a baseline for comparison. Then, the trial-averaged activity was fitted with the second-order polynomial functions (Methods).

To illustrate this analytical method using neural data from a representative animal, we classified M2 neurons into 3 groups: locomotion(+), locomotion(−), and unclassified. Based on their activity profiles during locomotion (Fig. 5A, B; Table 2). Locomotion(+) neurons exhibited consistently higher activity during locomotion, while locomotion(−) neurons showed sustained suppressed activity during the same period (Fig. 5C, D). After splitting each recording session into two halves of trials during locomotion, we found that most cells remained in the same response category across both halves of the trials (Supplementary Fig. 5A). Interestingly, there were more locomotion(−) neurons than locomotion(+) neurons across all three environmental contexts, and the percentages of the two types of neurons were also significantly higher than that of randomly shuffled data (Fig. 5E). In addition, the number of locomotion(−) neurons decreased from the running wheel to the Y maze and then to the open field (Fig. 5E). To further assess how locomotion(+) and locomotion(−) neurons are represented across different contexts, we compared the observed distribution to the randomly shuffled distribution, as previously described. We

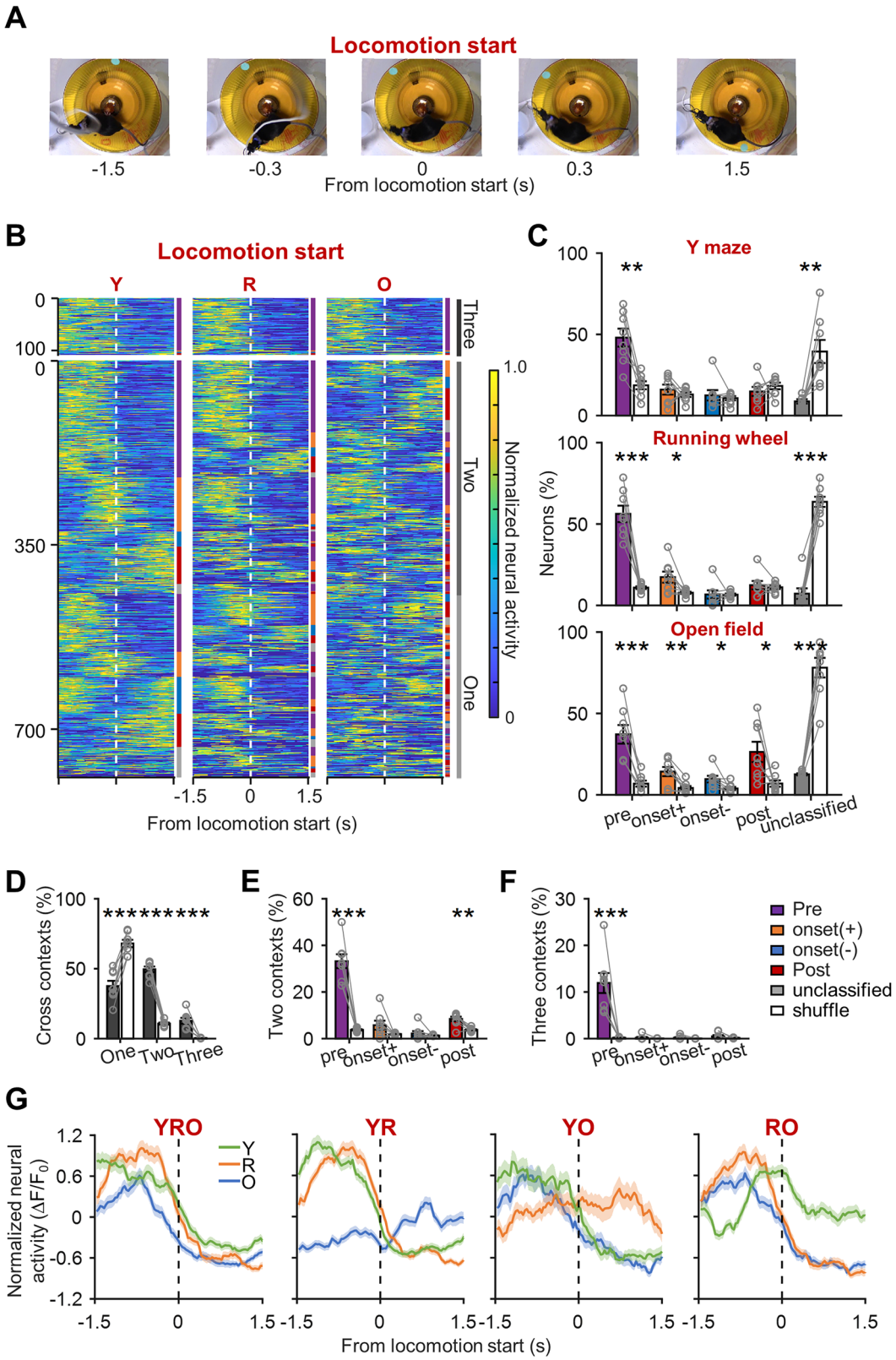

found that the cross-context representations of locomotion(−) neurons were significantly greater than expected by chance, whereas the proportion of cross-three-context locomotion(+) neurons was low (~1%), though still higher than expected by chance. In addition, the proportion of cross-two-context locomotion(+) neurons did not differ significantly from what was expected by chance (Fig. 5F, G). Overall, there are significantly more two or three-context locomotion(−) cells than locomotion(+) cells (Fig. 5H, I). The average activity profiles of these cross-context cells confirmed their designation as either locomotion(+) or locomotion(−) cells (Fig. 5J, K).

Additionally, to compare the second-order polynomial function-based classification scheme with an alternative method, we classified neurons based on their average activities in three time windows: before locomotion,

Fig. 3 | M2 neurons active before locomotion are over-represented across contexts. A Example video frames showing an animal's behavior close to the initiation of locomotion in the running wheel. **B** Raster plots showing trial-averaged activity of M2 neurons around locomotion start. The activity of individual neurons in each context was aligned by the onset of locomotion and averaged across trials. The cell sorting order was generated based on the timing of each cell's peak activity, averaged from odd-numbered trials in the Y-maze. This sorting order was then applied to the average activity from even-numbered trials in the Y-maze to validate the consistency of response patterns within a single context. The same sorting order was also applied to all trials in the Open Field and Running Wheel conditions, enabling consistent comparison across contexts. Furthermore, cells were grouped according to their ability to represent across contexts into three categories: cross-three-context neurons, cross-two-context neurons, and single-context neurons. Y, Y maze; R, running wheel; O, open field (same as below). Color bar on the right side of every raster plot showed the categories of every single neuron. Purple, Pre; orange, onset(+); blue, onset(−); red, Post; gray, unclassified (same as bar legend).Color bar on the far right showed classification of cross-context. Top panel (dark gray bar on the right), cross-three-context neurons; Bottom panel (light gray bar on the right), cross-two-context and single-context neurons. **C** Percentage of Pre, onset(+), onset(−), and Post neurons around locomotion start in the 3 contexts. $N = 8$ biologically independent animals. Pre: Y: $t = 5.05$, $p = 0.001$; R: $t = 8.56$, $p < 0.001$; O: $t = 6.25$, $p < 0.001$. **D** Percentage of neurons displaying similar activity in 1 (left, $t = -8.45$, $p < 0.001$), 2 (middle, $t = 18.49$, $p < 0.001$), or 3 (right, $t = 5.93$, $p = 0.001$) contexts. Randomly shuffled data were calculated based on the percentage of different neurons in (**C**) (see Methods). $N = 8$ biologically independent animals. **E** Percentage of Pre ($t = 10.28$, $p < 0.001$), onset(+) ($t = 1.93$, $p = 0.10$), onset(−) ($t = -0.85$, $p = 0.42$), and Post ($t = 4.50$, $p = 0.003$) neurons that are similarly active across the Y maze, running wheel, and open field conditions. $N = 8$ biologically independent animals. **F** Percentage of Pre ($t = 5.51$, $p < 0.001$), onset(+) ($t = 0.76$, $p = 0.47$), onset(−) ($t = 1.24$, $p = 0.26$), and Post ($t = 1.18$, $p = 0.28$) neurons that are similarly active across 2 behavioral conditions. $N = 8$ biologically independent animals. **G** Population activity of the cross-context cells for Pre neurons in the window of locomotion initiation. $N = 8$ biologically independent animals. Error bars represent the standard error. $^{*}p < 0.05$, $^{**}p < 0.01$, $^{***}p < 0.001$, paired t-test.

during locomotion and after locomotion. If the activity of a neuron during locomotion was significantly higher than the other two windows, the neuron was defined as locomotion(+) neuron. If the activity of a neuron during locomotion was significantly lower than the other two windows, the neuron was defined as locomotion(−) neuron. We found a similar group distribution of neurons to that classified by the second-order polynomial functions, as well as a similar abundance of locomotion(−) neurons and their cross-context representation (Supplementary Fig. 5B–F).

To further evaluate the relationship among locomotion start neurons [LST-Pre], locomotion stop neurons [LSP-Post], and sustained locomotion(+) and locomotion(−) neurons, we determined whether they belong to separate or overlapping populations. We found that most locomotion(−) neurons overlapped with either LST-Pre neurons, LSP-Post neurons, or both, although a subset of locomotion(–) neurons did not overlap with either the LST-pre or LSP-post categories (Fig. 6A, Supplementary Fig. 6). However, most locomotion(+) neurons did not overlap with LST-Pre neurons or LSP-Post neurons (Fig. 6B). These results also further suggested that more M2 neurons show sustained suppression than activation during locomotion in different contexts at the single-cell level.

To examine the similarity of neuronal activity in M2 during locomotion in different contexts at the population level, we analyzed M2 neuronal activity with principal component analysis (PCA)[35,36] (Fig. 6C). Although varied in amplitude, the first principal component displayed a similar temporal activation profile across different contexts, which was characterized by higher activity before locomotion start and after locomotion stop, and lower activity during movement (Fig. 6C). We then combined the first three PCAs together and calculated the pairwise correlation coefficients between different contexts. We found a high activity correlation across contexts, especially between the running wheel and Y maze (Fig. 6D). These results further indicated that M2 shows a similar locomotion start and stop-related activation pattern at the population level across different contexts. Interestingly, compared to the resting period, most M2 neurons displayed higher activity during locomotion (Supplementary Fig. 7). This result suggests that the suppressed activity during locomotion is relative to the start and stop periods, but still higher than the resting level. In summary, our results indicated that most cross-context neurons in the M2 region displayed suppressed activity during locomotion compared with the initiation and the termination of locomotion.

Limited representation of speed and acceleration in M2 neurons

Movement velocity is an intrinsic kinematic parameter during locomotion, which may be less affected by movement contexts. To test this hypothesis, we measured the velocity and acceleration in different contexts and found that mice ran faster in the running wheel than in the other 2 arenas (Fig. 7A). To identify speed-related neurons, we calculated Pearson's correlation (r, speed score) between neural activity and running speed (Fig. 7B, METHODS). Based on previous methods, the cells with speed scores higher than the 90th percentile of a shuffled distribution (lower: −0.44, upper: 0.45) were defined as speed cells (Fig. 7C). We found that ~8% of neurons were speed-responsive cells in individual arenas, which was close to the chance level (Fig. 7D). Few neurons (<1%) were found to stably encode speed under different behavioral conditions (Fig. 7E). The cluster analysis also demonstrated that speed neurons in different contexts were distinct from each other (Fig. 7F, Supplementary Fig. 8, Table 3). Similarly, some M2 neurons encoded acceleration (Fig. 7G) but few crossed different contexts (Fig. 7H, I). Therefore, contrary to our hypothesis, the representation of speed and acceleration may be limited in M2 and these neurons are mostly context-specific.

Discussion

In the present study, we used a second-order polynomial function to analyze the M2 activity in relationship to different locomotor control conditions (start, maintain, or stop)[34]. With this method, we systematically dissected the M2 activity during self-initiated locomotion under different contexts. We found that a large population of neurons in M2 signaled the initiation and termination of the locomotor behaviors, and this signal was stable across different contexts (Figs. 3 and 4). Furthermore, those neurons displayed suppressed activity during sustained movement in different contexts (Figs. 5 and 6). Conversely, most of the neurons in M2 activated by locomotion, were context-specific (Figs. 5 and 6).

Previous studies of cortical encoding of locomotion left open the important question whether M2 neurons encode the same type of locomotor control variables in different spatial contexts. Here, we introduced three environmental contexts in which the animal's locomotion is differently constrained. The mice were confined to run on a circular plate of the running wheel, or 3 linear arms of the Y maze, but were free to move in the open field. However, the animals in those conditions had several similar locomotor behaviors including: locomotion start, maintenance, stop, and resting. We found that M2 neurons encoded all of these motor control variables for self-initiated locomotion. Previous functional studies have found that rats with unilateral removal of M2 make fewer contralateral turns when running in a T-maze[37] and optogenetic stimulation in M2 induces circular running behavior in mice[38,39]. Furthermore, electrical microsimulation in M2 leads to a combination of eye, head, and vibrissa movements both contralaterally and ipsilaterally[12,27]. These results indicated that M2 is an essential hub to modulate different locomotor behaviors. However, those studies involved a single environmental context, and it is not known how M2 encoding of motor control variables changes with context. Our results provide direct insight into what type of locomotor variables are represented consistently in M2 across different environmental contexts. Strikingly, we found that the start and stop-modulated M2 neurons were less dependent on the contexts; the locomotion-activated neurons were context-specific. Our data demonstrate that M2 encodes self-initiated locomotion behaviors in both a context-dependent and a context-independent manner.

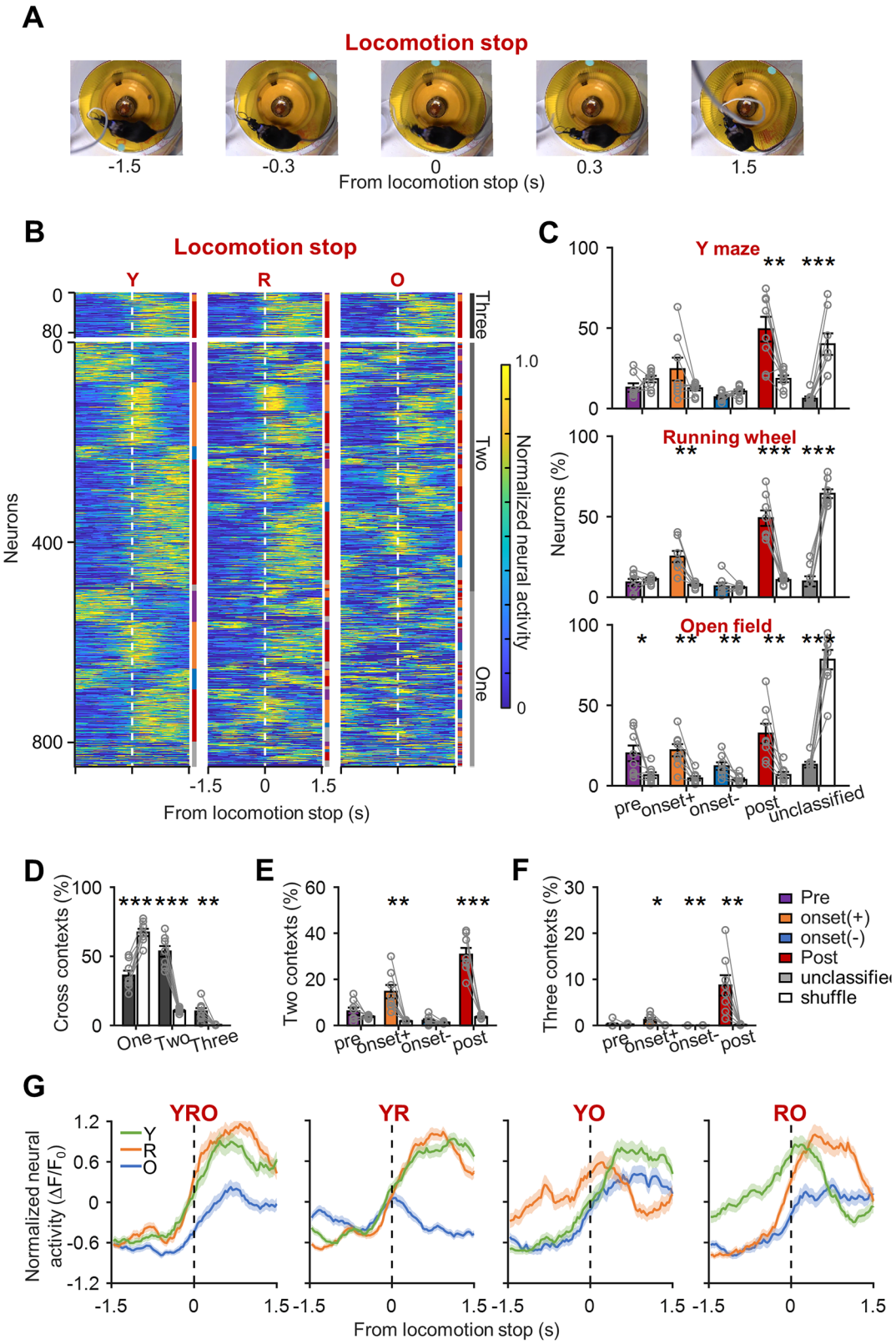

Our results demonstrated that a large proportion of superficial M2 neurons were active before the starting and after the ceasing of locomotion, and those neurons could be engaged cross different contexts. The control of start and stop is thought to be the traffic-related signal during locomotion[34], and this has been found in the reticulospinal[40] and several dopamine-related brain regions including the substantia nigra and striatum[34,41]. The neurons in those regions display increased or decreased activity before or after behavioral start and stop[41]. In addition, electrical or optogenetic stimulation of those regions may induce the initiation or cease of locomotion[3]. The M2 receives the dopaminergic input from the midbrain ventral tegmental area and substantia nigra[42,43] and reciprocally connects with the striatum. In addition, neurons in M2 show planning signals during locomotion[44] and

Fig. 4 | M2 neurons active after locomotion are over-represented across contexts. **A** Example video frames showing an animal's behavior close to locomotion stop in the running wheel. **B** Raster plots showing trial-averaged activity of M2 neurons around locomotion stop. The activity of individual neurons in the 3 contexts was aligned by locomotion stop and averaged across trials. The cell sorting order was generated using the same method as that for LST raster plots (Fig. 3B). Color bar on the right side shows the categories of every single neuron. Top, cross-three-context neurons, Bottom, cross-two-context or single-context neurons. **C** Percentage of Pre, onset(+), onset(−), and Post neurons in the time window of locomotion stop in the 3 contexts. $N = 8$ biologically independent animals. Post: Y: $t = 3.95$, $p = 0.006$; R: $t = 8.11$, $p < 0.001$; O: $t = 3.96$, $p = 0.005$. **D** Percentage of neurons displaying similar activity in 1 (left, $t = -7.27$, $p < 0.001$), 2 (middle, $t = 11.34$, $p < 0.001$), or 3 (right, $t = 4.13$, $p = 0.004$) contexts. $N = 8$ biologically independent animals. **E** Percentage of Pre ($t = 1.34$, $p = 0.22$), onset(+) ($t = 4.49$, $p = 0.003$), onset(−) ($t = 1.13$, $p = 0.30$), and Post ($t = 9.58$, $p < 0.001$) neurons that are similarly active across the Y maze, running wheel, and open field conditions. $N = 8$ biologically independent animals. **F** Percentage of Pre ($t = 0.01$, $p = 0.99$), onset(+) ($t = 2.64$, $p = 0.03$), onset(−) ($t = -4.99$, $p = 0.002$), and Post ($t = 3.86$, $p = 0.006$) neurons that are similarly active across 2 behavioral conditions. $N = 8$ biologically independent animals. **G** Population activity of the cross-context cells for Post neurons during locomotion stop. Error bars represent the standard error.

sensory cue-conditioned actions[12]. Our results showed that the peak activity in most M2 neurons was 0.3–1.5 s before movement initiation, which is earlier than the signal in the substantia nigra[41] and striatum[34], indicating that M2 may be the first hub to initiate the start signal during locomotion. The stop signal originated in the superficial layer of M2 occurs approximately 200 ms before the stop behaviors; however, the peak of most neurons fell into the window 0.3–1.5 s after locomotion stop. Thus, the timing of the stop signal in M2 appears to be later than that in the substantia nigra[41] and striatum[34]. Importantly, the over-represented start/stop signals in M2 were stable and occurred across different contexts, indicating that the start/stop signals in M2 may initiate from an innate drive that connects with start- and stop-related subcortical regions to control traffic-related behaviors.

Previous studies provided divergent views on how the motor cortex is modulated during sustained running. Wide-field imaging in rodents has found that most cortical regions including M2 have increased neural activity during continual running[45]. On the contrary, several other studies have found that neurons in the deep layer of the motor cortex display suppressed activity during locomotion compared with rest[46]. Interestingly, our results found that most superficial M2 neurons displayed higher activity during locomotion than in the rest period (Supplementary Fig. 7); however, they displayed decreased activity compared with the initiation and the termination of locomotion across different contexts (Figs. 5 and 6). During locomotion, sustained running may be correlated with the alternating activity in the spinal cord which serves to maintain the walking posture and gait. Although the neurons in M2 showed increased activity during locomotion, they displayed the highest activity at the initiation or termination of locomotion. These results supported the importance of M2 for motor planning during locomotion, but also suggested that M2 may play a lesser role in the maintenance of posture and gait.

In the present study, LST-pre, LSP-post, and locomotion(−) neurons were classified based on three distinct temporal segments extracted from the complete movement sequence, designed to separately capture local activity transitions and globally sustained activity patterns. For LST/LSP-related classification, neural signals were analyzed within a 3-s window centered on locomotion onset (1.5 s before to 1.5 s after; Supplementary Fig. 6A, B). This analysis revealed four distinct activity patterns: Pre, Onset(+), Onset(−), and Post (Fig. 2F). In contrast, locomotion(−) and locomotion(+) neurons were identified by analyzing activity across the entire duration of each locomotion episode—interpolated to 120 sample points to normalize for trial length variability—along with the 1.5-s windows preceding locomotion onset and following locomotion offset (Supplementary Fig. 6A, B). This classification focused on comparing overall activity during locomotion with that before and after movement, rather than emphasizing local transitions at movement boundaries. While some neurons clearly showed reduced activity during locomotion (i.e., locomotion(−)), their elevated activity before or after movement did not always align precisely with the LST-pre or LSP-post activity profiles during movement transition windows (Supplementary Fig. S6C–H). Instead, they can be better classified as LST-onset(+), LST-onset(−), LST-post, LSP-pre, LSP-onset (+), or LSP-onset(−). As a result, a subset of locomotion(−) neurons did not overlap with either the LST-pre or LSP-post categories (Fig. 6).

Neurons in the superficial layer of M2 receive visual, auditory, and somatosensory stimuli through cortical connections and display a preceding signal before sensory response[12]. In our task, different contexts had different sensory stimulation. The activity of some M2 neurons was different for the same locomotor behaviors in different contexts, which may be due to different sensory inputs in different environments. This hypothesis was confirmed by the different neural activation patterns for locomotion maintenance in different behavioral contexts. Furthermore, neurons in the superficial layer of M2 are connected with the dendritic trees of layer V projection neurons in M2, which may modulate the command signals of M2 corticospinal neurons. In addition, neurons in the superficial M2 send a projection to layer V of M1. Therefore, the different activation of M2 neurons in different contexts may modulate the command signal in M1 during locomotion; this is supported by the context-specific limb movement coding in M1[47]. The activity difference in different environmental contexts may be due to environmental constraints on behavioral variability.

The rodent M2 contains both the anterior/lateral and the most medial/dorsal portion of the frontal cortex[12]. It is functionally engaged in both skillful forelimb-grasping tasks and goal-directed locomotion tasks, as shown by electrophysiological recording and calcium imaging techniques in freely moving animals[19,48]. The function of M2 has also been studied in other animal models including cats[13,14] and non-human primates[15,16]. Compared with rodents, the M2 regions of the cat and the primate are larger in size, anatomically well separated from M1 and prefrontal cortex, and functionally act more like a higher-order brain region to modulate motor behaviors. Because non-human primates frequently use their forelimbs in dexterous tasks, previous primate research mainly investigated how M2 controls hand movements in restrained conditions with electrophysiological approaches, but rarely studied locomotor control in free-moving conditions[17]. On the other hand, cats walk with all four limbs and offer a great experimental model to analyze step cycles and their neural control. Particularly, electrophysiological studies in the cat M2 cortex have revealed neural activity patterns related to the planning of gait modification and interlimb coordination while stepping over obstacles on the ground[13,14].

Despite the differences in anatomy, behavior, and recording methods, M2 neurons in all three animal models display motor planning-related signals[12–15]. However, most of the previous studies were performed in a single behavioral context; how M2 neurons encode the same type of locomotor control variables in different environmental contexts is relatively unknown. Our results demonstrate that movement initiation and termination-related signals in M2 are largely independent of the behavioral contexts, but locomotion maintenance neural signals are mostly context-specific. The context-dependent locomotion-activated neurons may reflect differences in both sensory inputs and kinematic responses across contexts. In contrast, the abundance of context-independent start or stop neurons suggests robust encoding of egocentric motor planning signals in M2 that remains stable across the three environmental contexts. Thus, our results provide insights that M2 controls self-initiated locomotor behaviors in both context-dependent and context-independent manners.

There are certain limitations in the present study. Our study was designed to address how different environmental contexts modulate the neuronal responses of M2 in self-initiated locomotion. For this purpose, the camera was set over the top of the behavioral apparatus and far away from the animals to facilitate capturing the complete locomotor trajectories in

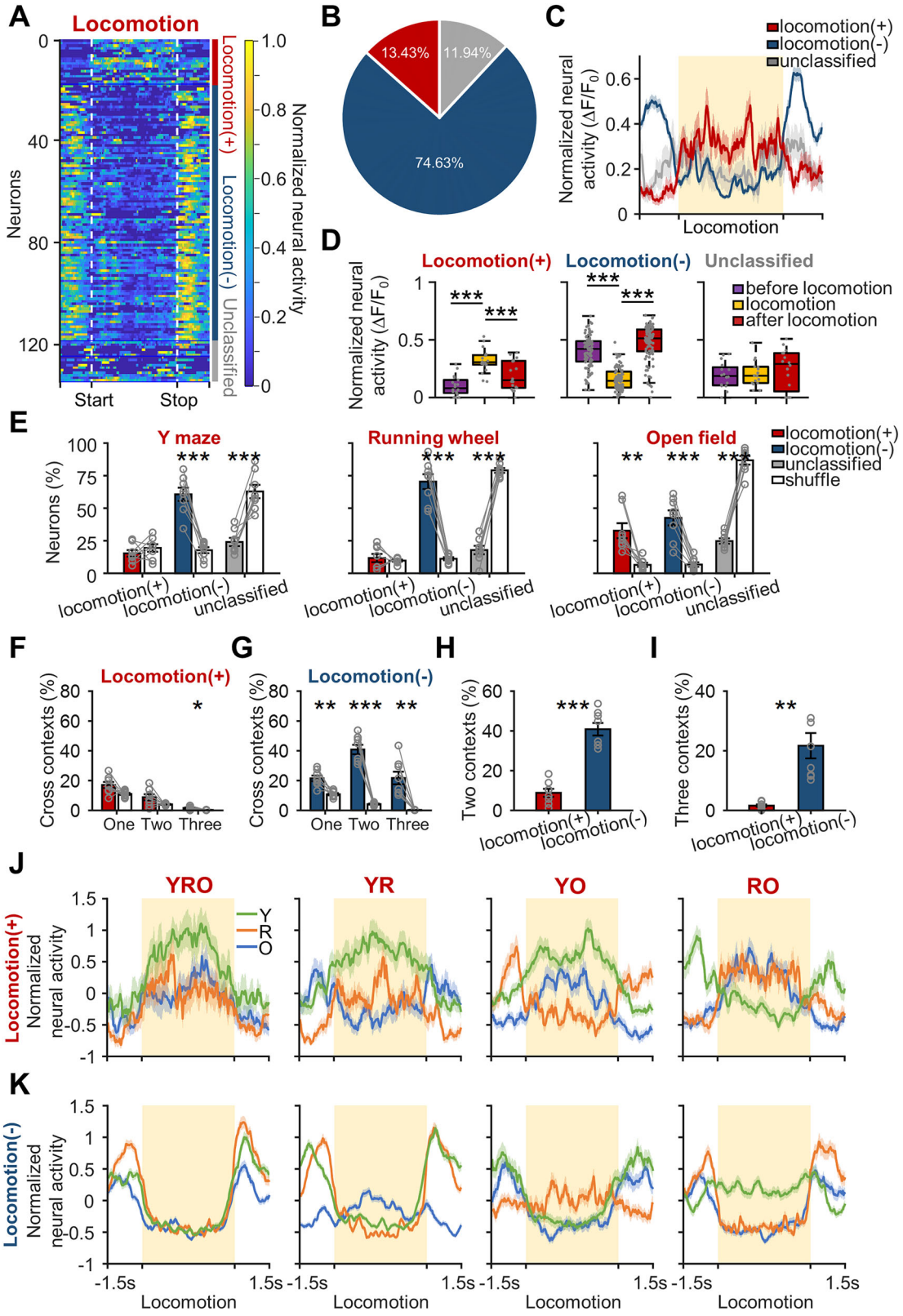

each of the three environmental contexts and a variety of start, stop, and locomotion events. However, this recording configuration did not support the detection of small turning angles or individual step cycles. Analyzing the step cycle in mice typically requires capturing behavioral videos from beneath the abdomen using a high-speed camera, but this setup poses challenges for experiments involving the running wheel and Y-maze. The step cycle in a mouse could be quite fast and up to more than 10 Hz, which is difficult to resolve by the Ca2+ imaging method used in the present study. Future studies with different recording methods could be conducted to address how different environments modulate different kinematic parameters, such as the step cycles, turning angles, and their neural correlates in the motor cortex.

Fig. 5 | M2 neurons show more sustained suppression than activation during linear locomotion. **A** Raster plot showing the activity of 134 neurons in an example animal during continuous running in the running wheel. The activity in different trials between locomotion start and stop was interpolated into 120 bins and 45 bins (1.5 s) of activity were added before and after locomotion. Then the activity of different neurons was averaged across trials. The trial-averaged activity of all neurons was fitted with the second-order polynomial function and sorted based on locomotion(+), locomotion(−) and unclassified (see Methods). **B** Percentage of locomotion(+), locomotion(−) and unclassified neurons in (**A**). **C** Averaged neural activity of the 3 groups of neurons in (**A**). **D** Averaged activity before/during/after locomotion of locomotion(+), locomotion(−) and unclassified neurons. Locomotion(+): $F = 19.18$, $p < 0.001$; Locomotion(−): $F = 151.72$, $p < 0.001$; Unclassified: $F = 0.652$, $p = 0.53$. $N = 134$ neurons of one sample animal. **E** Percentage of locomotion(+) (Y: $t = -0.99$, $p = 0.35$; R: $t = 0.49$, $p = 0.64$; O: $t = 3.90$, $p = 0.006$), locomotion(−) (Y: $t = 8.91$, $p < 0.001$; R: $t = 11.65$, $p < 0.001$; O: $t = 6.99$, $p < 0.001$) neurons during locomotor behaviors in the 3 arenas. $N = 8$ biologically independent animals. **F** Percentage of locomotion(+) neurons relative to the entire cell population across different cross-context conditions in 1 ($t = 2.34$, $p = 0.05$), 2 ($t = 2.15$, $p = 0.07$), or 3 ($t = 2.98$, $p = 0.02$) contexts, compared to the randomly shuffled data. $N = 8$ biologically independent animals. **G** Percentage of locomotion(−) neurons displaying similar activity in 1 ($t = 4.64$, $p = 0.002$), 2 ($t = 11.53$, $p < 0.001$), or 3 ($t = 5.10$, $p < 0.001$) contexts compared to the randomly shuffled data. **H** Percentage of locomotion(+) and locomotion(−) neurons that are similarly active across 2 behavioral conditions ($t = -7.59$, $p < 0.001$). $N = 8$ biologically independent animals. **I** Percentage of locomotion(+) and locomotion(−) neurons that are similarly active across the Y maze, running wheel and open field conditions ($t = -4.52$, $p = 0.003$). $N = 8$ biologically independent animals. Population activity of the cross-context cells for locomotion(+) (**J**) and locomotion(−) neurons (**K**). Error bars represent the standard error.

Table 2 | Functional classification criteria for sustained locomotion signals

Criteria	$p < 0.05$					$p > 0.05$
	a > 0		a < 0			
(−b/2a)	[Duration period]	Others	[Duration period]	Others	Active time <0.5	–
Classification	Locomotion(−)	unclassified	Locomotion(+)	unclassified	unclassified	unclassified

Taken together, this study has identified both context-dependent and context-independent locomotion-related neural signals in M2, which may collectively contribute to the control of self-initiated locomotion behaviors during navigation in different spatial contexts. This finding raises intriguing questions about the computational advantages of such a neural processing strategy. To navigate the complexities of real-world dynamics, an intelligent agent must continuously acquire, update, accumulate, and utilize knowledge throughout its operational lifespan[49]. In the context of continual learning in artificial intelligence (AI), the strategic preservation of specific parameters associated with prior knowledge can enhance the retention of existing information while facilitating the integration of new information, a process often described as balancing learning plasticity and memory stability[50,51]. This balance is critical for adaptive intelligence, enabling the effective acquisition of knowledge and skills, their continuous refinement through novel experiences, and their transferability across diverse domains. Our discovery of cross-text stability in M2 neural encoding mechanisms provides biologically inspired insights that may advance the understanding of this fundamental challenge in both neuroscience and AI research.

Methods

Animals

Adult male wild-type C57BL/6 mice (8–10 weeks, 20–25 g, $n = 8$) were used for imaging experiments. All experimental procedures were performed in compliance with animal protocols approved by the Institutional Animal Care and Use Committee at the National Institutes of Health and Zhejiang University. We have complied with all relevant ethical regulations for animal use.

Surgical procedures

The surgery was performed based on our previous methods[19,31,52,53]. Before surgery, the stereotaxic apparatus and surgical instruments were disinfected with 70% ethanol for 30 min. To relieve surgery-related edema and inflammation, the animal was anesthetized with sodium pentobarbital (0.15 ml/g, i.p.) and pre-treated with dexamethasone (0.2 mg/kg, i.p.). Then, the fur between the eyes and ears was trimmed and the skin was disinfected with clean swabs of 70% ethanol thrice. Next, an incision of ~4 mm was made over the secondary motor cortex, and 2% lidocaine was used locally (s.c.) to alleviate the acute pain during surgery. To prevent tissue growth and stabilize the coverslip, the periosteum was scraped off with a scalpel blade and the target craniotomy region was cleaned with 100% alcohol. After that, a high-speed microdrill (typically between 7000 and 10,000 rpm) with a 0.5 mm burr was used to create a circular craniotomy (slightly larger than 3 mm) around the desired viral injection location (AP: 1.8, ML: 0.5)[12,38,52,54]. Finally, AAV-hSyn-GCaMP6s were infused to the surface of the secondary motor cortex by a glass pipette with a tip size of ~0.3 mm based on our previous methods[31,55]. With this method, the approximate depth of the imaging plane relative to the cortical surface is about 200~300 μm, and regions-of-interest (ROIs) mostly coincide with the cell bodies in layer II/III of the cortex. After recovery from the infusion surgery (7–9 days), we affixed a camera baseplate above the injection region. 3 days after baseplate surgery, we took the animals to the imaging room for about 2 h/day for 3 days and pre-handled the animals to accommodate them to the environment and experimenters.

Calcium imaging in different contexts

To systematically dissect the neural encoding in the secondary motor cortex during locomotion behaviors, calcium imaging experiments were performed in 3 different behavioral contexts: Y-maze, running wheel and open field. Before recording, the mice were familiarized with the recording room for 60 min. Then, the mouse was held by a towel and a miniature microscope was attached to the baseplate on the head. The imaging was performed in sequence, from Y-maze to running wheel to open field and each imaging session lasted for 8 min (Figs. 1A and 2A). In the Y maze condition, the animal was placed at the end of one arm and towards the wall at the beginning of the task. In this context, animals only moved back and forth in the range of three arms and were required to make a choice at the center of the maze. In the running wheel, the animal was placed in the tangential direction of a 15 cm circular plate surrounded by tall Perspex walls. In this context, animals ran constantly and quickly to maintain balance on the tilted plate, and they could only move in two tangential directions of the circular plate. In the open field condition, the animal was placed in the center of a 45 cm × 45 cm square open field at the beginning of an experiment and allowed to freely explore for 8 min. In this context, the animal could run in any direction and take turns freely. Behavioral videos were captured by a top-viewed camera (1080p, 30 Hz, LimeLight) during imaging.

Imaging data processing and Ca^{2+} signal extraction

Ca^{2+} imaging was performed via the head-attached miniature microscope (Inscopix, version nVista 2.0; LED power: 0.6–1.0 mW; camera resolution: 1440 × 1080 pixels). The calcium data were acquired at 30 Hz using nVista HD software (Inscopix, version 2.1) and the field of view was ~900 × 650 μm^2 at 0.65 mm/pixel resolution. During imaging, the behavioral videos synchronized with the calcium imaging were recorded by a high-definition camera (30 Hz, 1080p, LimeLight) over 3 arenas.

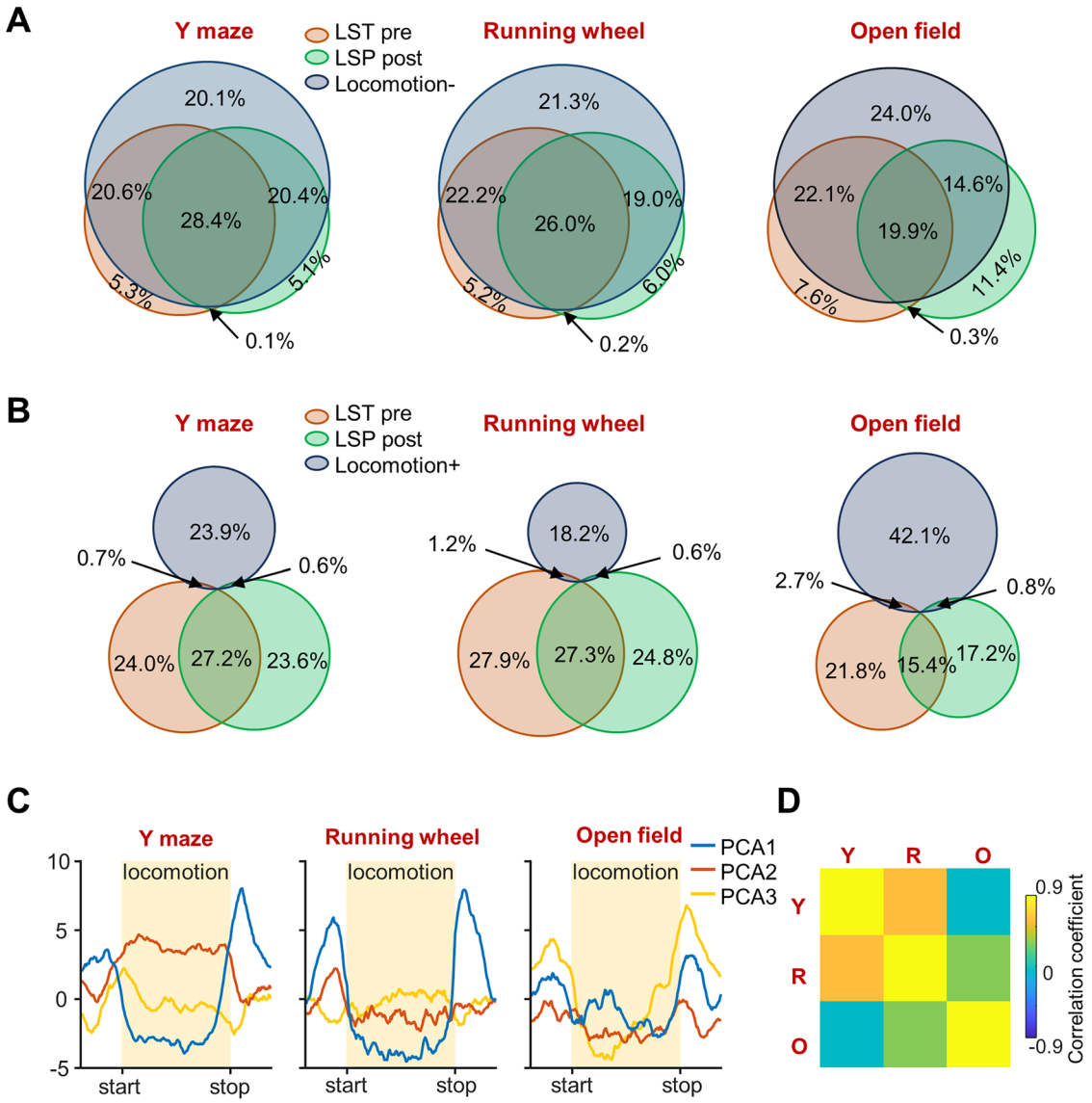

Fig. 6 | Relationship between locomotion neurons and start/stop neurons. **A** Venn diagrams showing the relationship between start/stop neurons and locomotion(−) neurons in different contexts. **B** Venn diagrams showing the relationship between start/stop neurons and locomotion(+) neurons in different contexts. **C** The temporal profiles of the first three principal components are derived from principal components (PCA) analysis of the neuronal population activity during locomotion in different contexts. Left, Y-maze; middle, running wheel; right, open field. **D** The matrix of pairwise linear correlation coefficients showing activation pattern similarities between different conditions. We combined the first three PCAs together and then calculated the Pairwise linear correlation coefficients between different conditions. Y, Y maze, R, Running wheel, O, Open field.

Ca^{2+} imaging videos were analyzed using the Image Processing Toolbox and custom-written scripts in MATLAB following published algorithms[11,19,31]. To reduce file size and data noise, raw videos were down-sampled four-fold along the spatial dimensions (Supplementary Movie, the video is shown after four-fold down-sampling). The three videos (Y-maze, running wheel and open field) of each animal were concatenated in time and motion artifacts were corrected using the 'stabilizer' plugin in ImageJ (NIH) or Imaging Data Processing Software (Inscopix). Then, the mean fluorescence intensity of each pixel was calculated during a recording session (~24 min) as F_0, and changes in pixel intensity at time t were expressed as $(F_t - F_0)/F_0$ or $\Delta F/F_0$.

To extract active neuronal Ca^{2+} signals, principal component and independent component analysis (PCA-ICA)[56] were applied to analyze the spatiotemporal data matrices of $\Delta F/F_0$ using the CellSort and fastICA toolboxes (freely downloadable from MATLAB Central)[57]. A spatiotemporal data matrix was decomposed into independent components based on the skewness of data distribution. After that, characteristic spatial filters were graphed and inspected, as well as the corresponding temporal signal of each component over the imaged area. In the present study, we focused our analysis on the Ca^{2+} event activity occurring in the fast-rising phase of a Ca^{2+} signal trace, which better matches the neuronal spiking activity than that in the slowly decaying phase[32] (Supplementary Fig. 3A–C). The detailed methods were described as follows: (1) reject the independent components contributed by blood flow, which have spatial filters overlapping with the dark shadows cast by blood vessels in the F_0 image; (2) reject the components with temporal skewness <1, because Ca^{2+} signals have a characteristic fast-rising and slow-decaying time course[56]; (3) for each selected component, identify the brightest spot (3 × 3 pixels) of the spatial filter as the location of the neuron and calculate the corresponding temporal signal from the $\Delta F/F_0$ video by subtracting the median value of the background area (ring-shaped outside the soma) from the average value of the soma area; (4) search for the rising phase of each Ca^{2+} event (peak $\Delta F/F_0 > 3$ standard deviations of baseline fluctuation) to identify periods of increased neuronal activity,

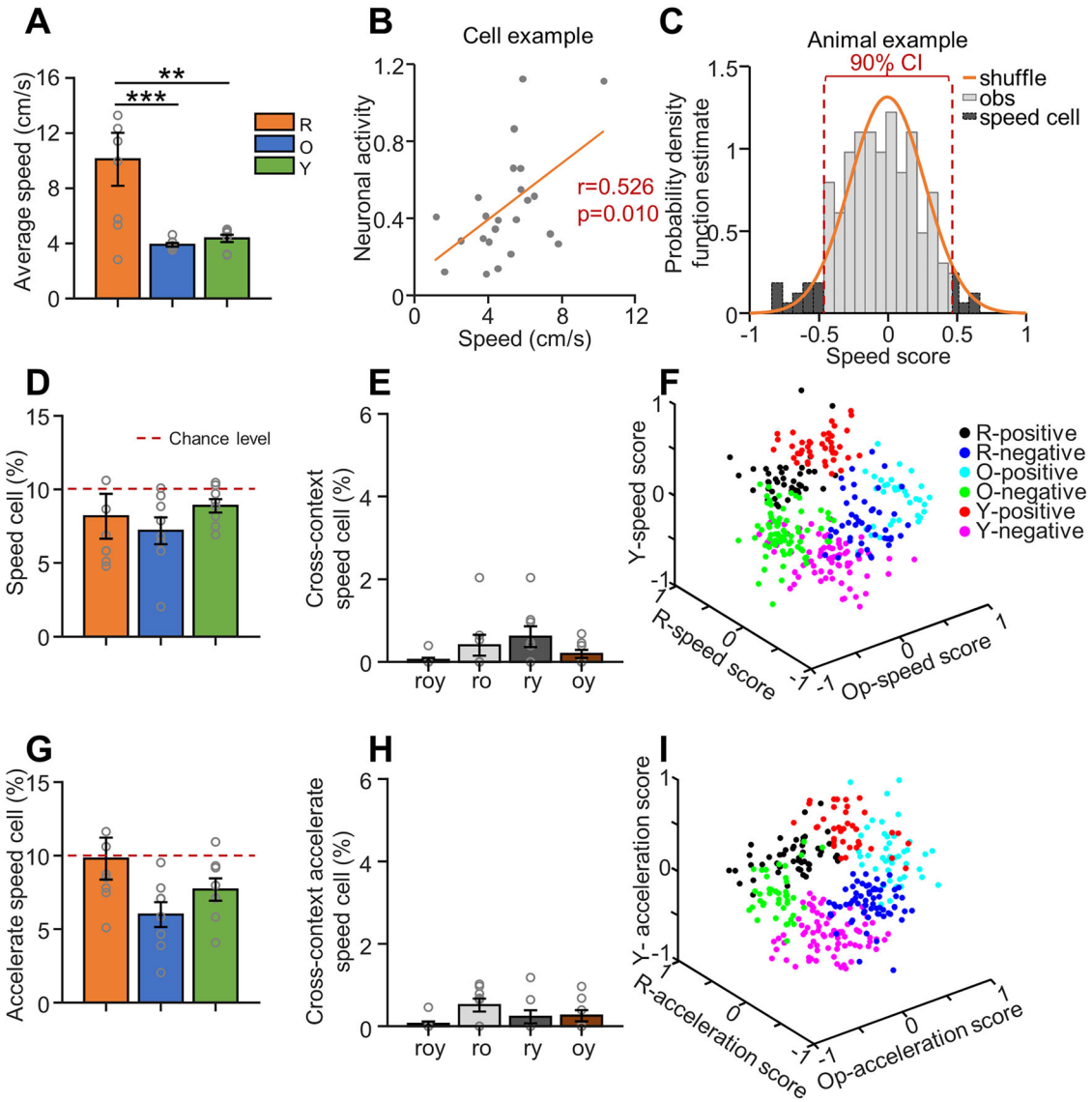

Fig. 7 | Limited representation of speed and acceleration in M2 neurons. **A** Average locomotor speed of mice in the 3 contexts. $N = 8$ biologically independent animals. $F = 9.486$, $p = 0.001$. **B** Scatterplot of neuronal activity and speed for an example neuron. Orange line: the linear fit between neuronal activity and speed ($r = 0.526$, $p = 0.010$). The calculated Pearson's correlation (r) was called the speed score. **C** Diagram showing the definition of speed cells based on previously published methods (see Methods). Orange line: probability density function calculated by shuffling 1000 times; red dashed line: the classification threshold (90th percentile of surrogate speed scores, lower: −0.44, upper: 0.45). Different blocks show distributions of speed scores of different cells. The cell with a speed score higher than the classification criterion was defined as a speed cell (dark gray blocks). **D** Percentage of speed cells in the 3 contexts. $N = 8$ biologically independent animals. $F = 0.648$, $p = 0.533$. Red dash line: chance level (same below). **E** Percentage of cross-context speed cells. **F** Distribution of speed score in different arenas. $N = 8$ biologically independent animals. We used the K-means algorithm to cluster the neurons and found the optimal number of clusters of all cells is 6 and their centers are well separated. **G** Percentage of acceleration cells in the 3 contexts. $N = 8$ biologically independent animals. $F = 3.278$, $p = 0.058$. **H** Percentage of cross-context acceleration cells. $N = 8$ biologically independent animals. **I** Distribution of acceleration score in different contexts. Error bars represent the standard error.

which has been shown to be closely associated with neuronal spiking activity. An automatic algorithm was used to detect the start of this rising phase when the 1st derivative of $\Delta F/F_0$ (calculated in a 200-ms moving window) rose above 0 and continued to increase above 5 standard deviations of baseline fluctuation, and the end of this rising phase was detected when the 1st derivative of $\Delta F/F_0$ fell below 0. Last, the spatial filters, calcium event signals, and trace signals together with behavioral data were separated into three files for further analysis.

Tracking of animal locomotion

The animal's locomotion in three arenas was tracked using our customized algorithm based on deep learning and a background subtraction algorithm – DeepBhvTracking[58]. Then, the position of the body center in each frame was obtained and instant speed was estimated by the Euclidean distance between two consecutive frames. Because the mice always move at the lowest level of the running wheel, a circular light-blue tag was stuck on the plate for tracking the actual speed of the mice.

Behavior analysis

To analyze the behavior-related neuronal activity, we defined animals' behavior through both manual and automatic methods. To automatically define an animal's locomotion and resting, 2 cm/s was used for the threshold based on previous methods[59]. Locomotion was defined when the speed of walking was higher than 2 cm/s and the duration was longer than 2 s. Resting was defined when the walking speed was less than 2 cm/s and the duration was longer than 2 s (Supplementary Fig. 2).

Table 3 | Cluster center of speed/acceleration cells in 3 arenas

Clusters	R	O	Y	Identify
Speed score				
1	0.539	−0.037	0.007	Positive speed cell in running wheel
2	−0.434	−0.011	−0.185	Negative speed cell in running wheel
3	−0.124	0.602	−0.147	Positive speed cell in open-filed maze
4	−0.074	−0.556	−0.036	Negative speed cell in open-filed maze
5	−0.009	−0.095	0.574	Positive speed cell in Y maze
6	−0.009	−0.107	−0.455	Negative speed cell in Y maze
Acceleration score				
1	0.533	−0.062	0.025	Positive acceleration cell in running wheel
2	−0.552	−0.026	−0.007	Negative acceleration cell in running wheel
3	0.010	0.649	0.046	Positive acceleration cell in open-filed maze
4	−0.013	−0.633	0.064	Negative acceleration cell in open-filed maze
5	−0.131	0.053	0.592	Positive acceleration cell in Y maze
6	0.006	−0.042	−0.589	Negative acceleration cell in Y maze

To better analyze the behavior-related neuronal activity, we also manually defined animals' behavior (locomotion, grooming, left/right turning, and resting) based on previous methods with some modifications[60]. Except for transient left/right turning behavior, the individual behavior should be longer than 2 s without other kinds of visible behavior in the middle (i.e., the time difference between the locomotion start and locomotion stop in a detected series was longer than 2 s). Locomotion was defined as an animal walking in the arena continuously and smoothly, with motionless state 1 s before and after locomotion (the center of the animal body should be unchanged for at least 1 s before and after locomotion). Grooming was defined as the animal's forelimbs lifted from the surface in a rising posture, including forepaw licking, nose/face stroking, stroking of the whiskers or forelimb fanning in front of the mouse. Resting was defined while four limbs of the animal stayed on the surface without obvious body movements and the duration was longer than 2 s. Some events that did not meet the criteria described above were excluded from further analysis and presented as unlabeled gaps. The locomotion, grooming, resting, turning and undefined behaviors together make up a total of 8 min.

Classification of neuronal activity using a second-order polynomial function

To examine the neural correlates of behavior, a frequently used method is to align neural activity traces to different behavior events, and then the activity level before and after an event is compared[19]. However, motor-related neural activity could occur in a dynamic and non-linear manner around a behavior event, such that a simple before-and-after contrast analysis would not capture the full range of neural dynamics[34]. To better evaluate the activity of individual neurons in different kinds of locomotion behaviors, we fit the neural activity around a behavioral event with a second-order polynomial function based on previous methods[34].

Before applying curve fitting, we used a 50% trial response threshold (requiring neurons to exhibit a significant neuronal response to locomotion in at least 50% of trials, evaluated by ΔF/F event which should be over 3 standard deviations of baseline fluctuation) to remove unstable neurons. As a result, 20–30% of neurons were excluded due to their unstable responses. Then, the activity of each neuron was first aligned by the time of locomotion start and averaged across trials. The trial-averaged neuronal activity was fitted with a second-order polynomial function as follows:

$$g(x) \sim ax^2 + bx + c$$

Where x is the time in seconds ($-1.5 \le x \le 1.5$), g(x) is the time-dependent normalized neural activity ($0 \le g(x) \le 1$), a is the quadratic coefficient of the polynomial function, b is the linear coefficient and c is the constant coefficient (Fig. 2F). The polynomial fit was considered significant if the p-value of this fit was lower than 0.05 and its R-squared was higher than 0.3. Given that we are only concerned with the relative changes in the amplitude of neural activity across different time windows during behavior, we do not further analyze the constant coefficient c.

Individual neurons with significant polynomial fit were classified into four activation profiles as follows: 1) if the quadratic coefficient is negative and the symmetry axis of the fitted polynomial function falls in the window of −1.5 s to −0.3 s, or the quadratic coefficient is positive and the symmetry axis of the fitted polynomial function falls in the window of 0.3 s to 1.5 s, the neuron was defined as a Pre neuron; 2) if the quadratic coefficient is negative and the symmetry axis falls in the window of 0.3 s to 1.5 s, or the quadratic coefficient is positive and the symmetry axis falls in the window of −1.5 s to −0.3 s, the neuron was defined as a Post neuron; 3) if the quadratic coefficient is negative and the symmetry axis falls in the window of −0.3 s to 0.3 s, the neuron was defined as an onset(+) neuron; 4) if the quadratic coefficient is positive and the symmetry axis falls in the window of −0.3 s to 0.3 s, the neuron was defined as onset(−) neuron.

In summary, the M2 neurons of each animal were divided into 5 groups according to the significance of polynomial fitting and the values of the quadratic and linear coefficients (see Fig. 2F and Table 1). The maximal activity of Pre neurons occurs 0.3 s to 1.5 s before a behavior event, while the maximal activity of Post neurons occurs 0.3 s to 1.5 s after a behavior event. Onset(+) and onset(−) neurons displayed maximal or minimal activity, respectively, between −0.3 s and 0.3 s. The neurons with non-significant polynomial fit or rarely active were excluded from further analysis (unclassified). With this method, one neuron cannot be classified into multiple groups.

To further evaluate the stability of locomotion-related neuronal responses, we split each recording session into two halves. The cell sequence in the second half was identical to that in the first half. We found that most cells maintained the same response category across both halves.

In addition to transient behavioral events such as locomotion start and locomotion stop, we analyzed neural activity patterns related to sustained locomotion, which occurred with varying durations in different trials. For standardization, we interpolated the neural activity traces in each bout of sustained locomotion with 120 sampling points, which corresponded to the median duration of locomotion bouts (4 s at 30 Hz). Then, we appended 1.5 s (45 sampling points) of neuronal activity before and after sustained locomotion. Finally, we used the second-order polynomial function to fit the standardized neural activity traces. Based on the sign of the quadratic coefficient and the location of the symmetry line of the fitted polynomial function, the neurons were divided into 3 groups: locomotion(+), locomotion(−) and unclassified (see Fig. 5A and Table 2). Locomotion(+) neurons displayed the highest activity during the locomotion window. Locomotion(−) neurons showed the lowest activity during the locomotion window. The unclassified group contained neurons with non-significant polynomial fit or rarely active (less than 0.5 s or 15 sampling points out of 210 in the standardized activity trace).

To further compare the second-order polynomial function-based classification scheme with an alternative method, we directly classified the neurons by comparing the average neural activity in different time windows. For the start/stop-related signals, we defined three activity windows (−1.5 s to −0.3 s, −0.3 to 0.3 s, and 0.3 s to 1.5 s). Then we calculated the average activity in each of the three windows and performed a t-test to compare between each pair of windows. If the activity in the window of −1.5 s to −0.3 s was significantly higher than that in the other two windows, the neuron was defined as Pre neuron. If the activity in the window of 0.3 s to

1.5 s was significantly higher than that in the other two windows, the neuron was defined as Post neuron. If the activity in the window of −0.3 s to 0.3 s was significantly higher than that in the other two windows, the neuron was defined as onset(+) neuron. If the activity in the window of −0.3 s to 0.3 s was significantly lower than that in the other two windows, and the activity difference between −1.5 s to −0.3 s and 0.3 s to 1.5 s was less 20%, the neuron was defined as onset(−) neuron. Otherwise, the neurons were defined as Pre or Post neurons. We found this method showed similar percentages of different groups of neurons compared to those classified by second-order polynomial functions (Supplementary Fig. 3D–F and Supplementary Fig. 5 and Figs. 2 and 5).

Definition of cross-context cells

After classifying the neurons into different functional groups, we inquired whether individual neurons encoded the same variables in three different behavioral contexts. If a neuron was classified into the same group in all three contexts, the neuron was identified as a cross-three-context neuron (e.g. a neuron was identified as Pre neuron in all Y maze, running wheel and open field conditions). If a neuron was classified into the same group in two behavioral contexts, the neuron was identified as a cross-two-context neuron. Last, if a neuron was classified into different groups at 3 behavioral contexts, then the neuron was defined as a single-condition neuron. In this analysis, if a cell was assigned to an unclassified group by fitting second-order polynomial function in all 3 arenas, it was excluded from further analysis. Cells assigned to the unclassified group in 2 behavior conditions were defined as single-condition cells.

To further explore whether cross-context activity occurs randomly in the M2 region, we shuffled the neural activity of M2 and calculated cross-context neurons in shuffled data. Following previous methods[59,61], we randomly and circularly shifted the neural activity of each neuron for 100 times. With this method, the correlation between neuronal activity and locomotion behavior was disrupted while the time-sequence information of activity was preserved. Then, we classified neurons into specific functional groups by the second-order polynomial fit method and defined cross-context cells using the above method. Last, we compared the statistical difference between experimental and shuffled proportions of cross-context neurons using paired *t-test*.

Principal component analysis

We also used principal component analysis (PCA) to study the neural space trajectory of M2 activity as mice performed locomotion. We combined the trial-averaged population activity across mice and projected them onto main PCA dimensions across 3 behavioral contexts. We then examined the correlational structure of M2 activity tuned to different behavior events between different behavioral contexts.

Speed score and speed cell definitions

Speed cells were defined based on prior methods[59,61]. To avoid interference by other behaviors, we restricted our analysis to those of manually selected locomotion segments (buff block in Fig. 1B). Then, the amplitude of each Ca^{2+} event in the locomotion segments was averaged and the average speed in each Ca^{2+} event time window was calculated. Last, we calculated Pearson's product-moment correlation coefficient (speed score) between the averaged amplitude of the Ca^{2+} event and the averaged speed. For each neuron, we also randomly circularly shifted the neural activity of each neuron for 1000 repetitions to calculate the shuffled speed score. The speed scores of the shuffled data in individual animals were pooled together and the 90th percentile of the distribution was used as a classification threshold. As shown in Fig. 7, speed cells were defined as neurons whose absolute speed score was greater than the classification criterion. Acceleration cells were defined using a similar method.

Histology

To confirm the expression of GCaMP6s in the secondary motor cortex, we anesthetized the animal with pentobarbital and perfused it with saline and 4% paraformaldehyde. Then, we fixed the brain with 4% paraformaldehyde for 24 h and immersed it with 15–30% sucrose. Next, we cut the tissue into coronal sections at 30 μm on a cryostat microtome (Leica CM1950, Germany) and mounted the slices on glass slides with coverslips. Then, we scanned the tissue with a Leica SP8 confocal laser-scanning microscope (Leica Microsystems, Germany) using 10× and 20× objectives, hybrid (HyD) detectors for sensitive detection, and sequential scan mode. As shown in Fig. 2D, most GCaMP-positivize neurons were annulus, indicating that they were healthy for imaging.

Statistics and reproducibility

$N = 8$ biologically independent animals were used in the present studies. Error bars in all figures represent mean ± SEM, the number (n) of samples employed is indicated in figure legends. The differences of locomotion behaviors among 3 contexts were tested using one-way ANOVA, followed by LSD test for multiple comparisons. The differences between experimental and shuffled data were analyzed using paired *t-test*. *indicates $p < 0.05$, **indicates $p < 0.01$, ***indicates $p < 0.001$.

Lead contact

Further information and requests for original data and analysis procedures should be directed to and will be fulfilled by the lead contact, Xinjian Li (lxjbio@zju.edu.cn).

Reporting summary

Further information on research design is available in the Nature Portfolio Reporting Summary linked to this article.

Data availability

Quantitative data and source data are provided supporting this study are available within the paper and Supplementary Materials (Supplementary Data 1). Raw data or source files are available from the LXJ on reasonable request.

Code availability

The custom code supporting this study are available within Supplementary codes.

Received: 1 October 2024; Accepted: 2 May 2025;
Published online: 10 May 2025

References

1. Nathan, R. et al. A movement ecology paradigm for unifying organismal movement research. *Proc. Natl Acad. Sci. USA* **105**, 19052–19059 (2008).
2. Herbert, E., Ouerdane, H., Lecoeur, P., Bels, V. & Goupil, C. Thermodynamics of animal locomotion. *Phys. Rev. Lett.* **125**, 228102 (2020).
3. Ferreira-Pinto, M. J., Ruder, L., Capelli, P. & Arber, S. Connecting circuits for supraspinal control of locomotion. *Neuron* **100**, 361–374 (2018).
4. Klaus, A., Alves da Silva, J. & Costa, R. M. What, if, and when to move: basal ganglia circuits and self-paced action initiation. *Annu. Rev. Neurosci.* **42**, 459–483 (2019).
5. Kiehn, O. Decoding the organization of spinal circuits that control locomotion. *Nat. Rev. Neurosci.* **17**, 224–238 (2016).
6. Arber, S. & Costa, R. M. Networking brainstem and basal ganglia circuits for movement. *Nat. Rev. Neurosci.* **23**, 342–360 (2022).
7. Taube, J. S. The head direction signal: origins and sensory-motor integration. *Annu. Rev. Neurosci.* **30**, 181–207 (2007).
8. Yang, J.-H. & Kwan, A. C. Secondary motor cortex: broadcasting and biasing animal's decisions through long-range circuits. *Int. Rev. Neurobiol.* **158**, 443–470 (2021).
9. Pirondini, E. et al. EEG topographies provide subject-specific correlates of motor control. *Sci. Rep.* **7**, 13229 (2017).

10. Allali, G. et al. Brain imaging of locomotion in neurological conditions. *Neurophysiol. Clin.* **48**, 337–359 (2018).
11. Peters, A. J., Chen, S. X. & Komiyama, T. Emergence of reproducible spatiotemporal activity during motor learning. *Nature* **510**, 263–267 (2014).
12. Barthas, F. & Kwan, A. C. Secondary motor cortex: where 'sensory' meets 'motor' in the rodent frontal cortex. *Trends Neurosci.* **40**, 181–193 (2017).
13. Nakajima, T., Fortier-Lebel, N. & Drew, T. Premotor cortex provides a substrate for the temporal transformation of information during the planning of gait modifications. *Cereb. Cortex* **29**, 4982–5008 (2019).
14. Nakajima, T., Fortier-Lebel, N. & Drew, T. A secondary motor area contributing to interlimb coordination during visually guided locomotion in the cat. *Cereb. Cortex* **33**, 290–315 (2022).
15. Cisek, P. & Kalaska, J. F. Neural correlates of reaching decisions in dorsal premotor cortex: specification of multiple direction choices and final selection of action. *Neuron* **45**, 801–814 (2005).
16. Graziano, M. The organization of behavioral repertoire in motor cortex. *Annu. Rev. Neurosci.* **29**, 105–134 (2006).
17. Foster, J. D. et al. A freely-moving monkey treadmill model. *J. Neural Eng.* **11**, 046020 (2014).
18. Nelson, A. et al. A circuit for motor cortical modulation of auditory cortical activity. *J. Neurosci.* **33**, 14342–14353 (2013).
19. Wang, X. et al. Deconstruction of corticospinal circuits for goal-directed motor skills. *Cell* **171**, 440–455.e414 (2017).
20. Fu, Y. et al. A cortical circuit for gain control by behavioral state. *Cell* **156**, 1139–1152 (2014).
21. Dadarlat, M. C. & Stryker, M. P. Locomotion enhances neural encoding of visual stimuli in mouse V1. *J. Neurosci.* **37**, 3764–3775 (2017).
22. Li, Y., Wang, X., Li, Z., Chen, J. & Qin, L. Effect of locomotion on the auditory steady state response of head-fixed mice. *World J. Biol. Psychiatry* **22**, 362–372 (2021).
23. McBride, E. G., Lee, S. J. & Callaway, E. M. Local and global influences of visual spatial selection and locomotion in mouse primary visual cortex. *Curr. Biol.* **29**, 1592–1605.e1595 (2019).
24. Christensen, A. J. & Pillow, J. W. Reduced neural activity but improved coding in rodent higher-order visual cortex during locomotion. *Nat. Commun.* **13**, 1676 (2022).
25. Kaneko, M., Fu, Y. & Stryker, M. P. Locomotion Induces Stimulus-Specific Response Enhancement in Adult Visual Cortex. *J. Neurosci.* **37**, 3532–3543 (2017).
26. Kaneko, M. & Stryker, M. P. Sensory experience during locomotion promotes recovery of function in adult visual cortex. *Elife* **3**, e02798 (2014).
27. Donoghue, J. P. & Wise, S. P. The motor cortex of the rat: cytoarchitecture and microstimulation mapping. *J. Comp. Neurol.* **212**, 76–88 (1982).
28. Gabbott, P. L., Warner, T. A., Jays, P. R., Salway, P. & Busby, S. J. Prefrontal cortex in the rat: projections to subcortical autonomic, motor, and limbic centers. *J. Comp. Neurol.* **492**, 145–177 (2005).
29. Reep, R. L. & Corwin, J. V. Topographic organization of the striatal and thalamic connections of rat medial agranular cortex. *Brain Res* **841**, 43–52 (1999).
30. Zingg, B. et al. Neural networks of the mouse neocortex. *Cell* **156**, 1096–1111 (2014).
31. Li, X. et al. Skin suturing and cortical surface viral infusion improves imaging of neuronal ensemble activity with head-mounted miniature microscopes. *J. Neurosci. Methods* **291**, 238–248 (2017).
32. Chen, T. W. et al. Ultrasensitive fluorescent proteins for imaging neuronal activity. *Nature* **499**, 295–300 (2013).
33. Lyu, C. et al. Deconstruction of vermal cerebellum in ramp locomotion in mice. *Adv. Sci. (Weinh.)* **10**, e2203665 (2022).
34. Sales-Carbonell, C. et al. No discrete start/stop signals in the dorsal striatum of mice performing a learned action. *Curr. Biol.* **28**, 3044–3055.e3045 (2018).
35. Ahrens, M. B. et al. Brain-wide neuronal dynamics during motor adaptation in zebrafish. *Nature* **485**, 471–477 (2012).
36. Mazor, O. & Laurent, G. Transient dynamics versus fixed points in odor representations by locust antennal lobe projection neurons. *Neuron* **48**, 661–673 (2005).
37. Cowey, A. & Bozek, T. Contralateral 'neglect' after unilateral dorsomedial prefrontal lesions in rats. *Brain Res.* **72**, 53–63 (1974).
38. Cao, V. Y. et al. Motor Learning Consolidates Arc-Expressing Neuronal Ensembles in Secondary Motor Cortex. *Neuron* **86**, 1385–1392 (2015).
39. van der Zouwen, C. I. et al. Freely behaving mice can brake and turn during optogenetic stimulation of the mesencephalic locomotor region. *Front. Neural Circuits.* **15**, https://doi.org/10.3389/fncir.2021.639900 (2021).
40. Juvin, L. et al. A specific population of reticulospinal neurons controls the termination of locomotion. *Cell Rep.* **15**, 2377–2386 (2016).
41. Jin, X. & Costa, R. M. Start/stop signals emerge in nigrostriatal circuits during sequence learning. *Nature* **466**, 457–462 (2010).
42. Bjorklund, A. & Dunnett, S. B. Dopamine neuron systems in the brain: an update. *Trends Neurosci.* **30**, 194–202 (2007).
43. Beier, K. T. et al. Circuit architecture of VTA dopamine neurons revealed by systematic input-output mapping. *Cell* **162**, 622–634 (2015).
44. Zhang, C. L. et al. Inhibitory control of synaptic signals preceding locomotion in mouse frontal cortex. *Cell Rep.* **37**, 110035 (2021).
45. West, S. L. et al. Wide-field calcium imaging of dynamic cortical networks during locomotion. *Cereb. Cortex* **32**, 2668–2687 (2022).
46. Pernía-Andrade, A. J., Wenger, N., Esposito, M. S. & Tovote, P. Circuits for state-dependent modulation of locomotion. *Front. Hum. Neurosci.* **15**, 745689 (2021).
47. Omlor, W. et al. Context-dependent limb movement encoding in neuronal populations of motor cortex. *Nat. Commun.* **10**, 4812 (2019).
48. Sul, J. H., Jo, S., Lee, D. & Jung, M. W. Role of rodent secondary motor cortex in value-based action selection. *Nat. Neurosci.* **14**, 1202–1208 (2011).
49. Hadsell, R., Rao, D., Rusu, A. A. & Pascanu, R. Embracing change: continual learning in deep neural networks. *Trends Cogn. Sci.* **24**, 1028–1040 (2020).
50. Parisi, G. I., Kemker, R., Part, J. L., Kanan, C. & Wermter, S. Continual lifelong learning with neural networks: a review. *Neural Netw.* **113**, 54–71 (2019).
51. Wang, L., Zhang, X., Su, H. & Zhu, J. A comprehensive survey of continual learning: theory, method and application. *IEEE Trans. Pattern Anal. Mach. Intell.* **46**, 5362–5383 (2024).
52. Mastwal, S. et al. Adolescent neurostimulation of dopamine circuit reverses genetic deficits in frontal cortex function. *bioRxiv*, https://doi.org/10.1101/2023.02.03.526987 (2023).
53. Sun, H. et al. Conjunctive processing of spatial border and locomotion in retrosplenial cortex during spatial navigation. *J. Physiol*. https://doi.org/10.1113/JP286434 (2024).
54. Manago, F. et al. Genetic disruption of Arc/Arg3.1 in mice causes alterations in dopamine and neurobehavioral phenotypes related to schizophrenia. *Cell Rep.* **16**, 2116–2128 (2016).
55. Liu, Y. et al. Touch and tactile neuropathic pain sensitivity are set by corticospinal projections. *Nature* **561**, 547–550 (2018).
56. Mukamel, E. A., Nimmerjahn, A. & Schnitzer, M. J. Automated analysis of cellular signals from large-scale calcium imaging data. *Neuron* **63**, 747–760 (2009).
57. Hyvarinen, A. & Oja, E. Independent component analysis: algorithms and applications. *Neural Netw.* **13**, 411–430 (2000).

58. Sun, G. et al. DeepBhvTracking: a novel behavior tracking method for laboratory animals based on deep learning. *Front. Behav. Neurosci.* **15**, 750894 (2021).
59. Kropff, E., Carmichael, J. E., Moser, M. B. & Moser, E. I. Speed cells in the medial entorhinal cortex. *Nature* **523**, 419–424 (2015).
60. Dombeck, D. A., Graziano, M. S. & Tank, D. W. Functional clustering of neurons in motor cortex determined by cellular resolution imaging in awake behaving mice. *J. Neurosci. Off. J. Soc. Neurosci.* **29**, 13751–13760 (2009).
61. Gois, Z. & Tort, A. B. L. Characterizing speed cells in the rat hippocampus. *Cell Rep.* **25**, 1872–1884.e1874 (2018).

Acknowledgements

This work was supported by the National Key Research and Development Program of China (2023YFB4705500), the National Natural Science Foundation of China (32371074, 32170991), the National Science and Technology Innovation 2030 Major Program (2022ZD0205000), the National Key R&D Program of China (2018YFC1005003), the Non-profit Central Research Institute Fund of Chinese Academy of Medical Sciences (2023-PT310-01) and the MOE Frontier Science Center for Brain Science & Brain-Machine Integration, Zhejiang University. A part of the research was supported by the Intramural Research Program of the National Institute of Mental Health, USA (ZIA MH002897 to KHW). We thank Bi Chao and Hong Xiaoli from the Core Facilities, Zhejiang University School of Medicine for their technical support.

Author contributions

Study conception and design: L.X.J., K.H.W. Experiments performing and data collection: L.X.J., C.R.L., F.L.Z. Visualization and data analysis: S.G.L., L.X.J., Y.C.C., L.M.X., L.C.F., L.Y.X., S.H. Funding acquisition: L.X.J., K.H.W., G.L.X. Project administration: L.X.J., K.H.W., G.L.X. Supervision: L.X.J., K.H.W., G.L.X. Results were discussed and interpreted by: L.X.J., K.H.W., S.G.L., Y.C.C. Manuscript was written and discussed by: L.X.J., K.H.W., S.G.L., G.L.X.

Competing interests

The authors declare no competing interests.

Additional information

Supplementary information The online version contains supplementary material available at https://doi.org/10.1038/s42003-025-08169-7.

Correspondence and requests for materials should be addressed to Kuan Hong Wang or Xinjian Li.

Peer review information *Communications Biology* thanks Elvira Pirondini and the other, anonymous, reviewer for their contribution to the peer review of this work. Primary Handling Editor: Jasmine Pan. A peer review file is available.

[1]Department of Neurology of the Second Affiliated Hospital, Interdisciplinary Institute of Neuroscience and Technology, Zhejiang University School of Medicine, and Key Laboratory of Medical Neurobiology of Zhejiang Province, Hangzhou 310020, PR China. [2]Nanhu Brain-computer Interface Institute, Hangzhou 311100, PR China. [3]McGovern Institute of Brain Research, Tsinghua University, 100084 Beijing, PR China. [4]NHC and CAMS Key Laboratory of Medical Neurobiology, MOE Frontier Science Center for Brain Science and Brain-machine Integration, School of Brain Science and Brain Medicine, Zhejiang University, Hangzhou 310058, PR China. [5]Shanghai Ping He School, Shanghai, PR China. [6]Key Laboratory of Biomedical Engineering of Ministry of Education, College of Biomedical Engineering and Instrument Science, Zhejiang University, Hangzhou 310027, PR China. [7]Unit on Neural Circuits and Adaptive Behaviors, National Institute of Mental Health, National Institutes of Health, Bethesda, MD 20892, USA. [8]Department of Neuroscience, Del Monte Institute for Neuroscience, University of Rochester Medical Center, Rochester, NY 14642, USA. [9]Key Laboratory of Medical Neurobiology of Zhejiang Province, Hangzhou 310020, PR China. [10]These authors contributed equally: Guanglong Sun, Chencen Yu, Ruolan Cai. [11]These authors jointly supervised this work: Kuan Hong Wang, Xinjian Li. ✉e-mail: kuanhong_wang@urmc.rochester.edu; lxjbio@zju.edu.cn